Effects of gelation on spinodal decomposition kinetics in gelatin

Rama Bansil* and Jyotsana Lal†
Center for Polymer Studies and Department of Physics, Boston University, Boston, MA 02215, USA

and Bruce L. Carvalho
Department of Materials Science and Engineering, Massachusetts Institute of Technology, Cambridge, MA 02139, USA
(Received 22 March 1991; accepted 18 July 1991)

We have studied the kinetics of spinodal decomposition in a gelatin–water–methanol mixture, which undergoes a sol–gel transition simultaneously with phase separation, using light scattering techniques. The kinetics of the sol–gel transition was investigated using falling-ball microviscometry techniques. We found that the kinetics of phase separation depend very strongly on temperature; and for deep quenches, where the rates of phase separation and gelation are comparable, the phase-separation process does not go to completion. Prior to the onset of gelation the initial growth rate of the structure factor can be described according to the Cahn–Hilliard model, even though the wavevector at maximum scattered intensity decreases as $k_m \sim t^{-0.6}$. For deep quenches after the onset of gelation, k_m remains unchanged with time, while the peak intensity exhibits a slow growth. The final domain size, k_{final}^{-1}, at which the phase-separating morphology becomes pinned decreases with increasing quench depth. Micrographs of the phase-separated domains reveal a connected structure on length scales of a hundred micrometres superimposed on a finer network structure due to gelation.

(Keywords: kinetics; spinodal decomposition; gelation; phase separation; gelatin)

INTRODUCTION

The kinetics of nucleation and spinodal decomposition[1,2] processes in phase-separating systems control the morphology of the material being fabricated and thus have a direct impact on the structure and properties of the product. For example, in the preparation of polymeric foams[3] phase separation is induced by adding a non-solvent or by lowering the temperature of the solution. The solvent is then removed by extraction or sublimation. A given microcellular foam morphology can only be realized by understanding the phase-separation kinetics of the polymer solution. If other processes such as aggregation, chemical crosslinking or gelation occur simultaneously with phase separation, then the phase-separated structure could be pinned at an intermediate stage of phase separation.

Since the rate of binary phase separation depends on polymer diffusion and since gelation or aggregation does slow down polymer diffusion, it is likely that the onset of gelation may drastically slow down the kinetics of the phase separation. Thus, the simultaneous occurrence of gelation and phase separation may provide another way to control the morphology of a polymeric product by inducing crosslinking during the phase-separation process. Conversely, since the location of the physical gel point depends on the concentration, it is also possible that phase separation itself might induce gelation. Physical gelation of atactic polystyrene solutions has been produced by this method[4]. Another application where the coupling of phase separation and gelation plays a crucial role is the process of immersion precipitation[5] to prepare polymeric membranes.

In recent years several studies of the kinetics of phase separation in polymer blends and polymer solutions[6,7] have been published. Phase-separation kinetics have also been measured in a covalently crosslinked hydrogel of *N*-isopropylacrylamide[8]. Hashimoto *et al.*[9] have shown that the morphology of slowly growing phase-separated domain structures in mixtures of polyisoprene and styrene–butadiene random copolymer containing 15% styrene could be pinned by inducing a chemical crosslinking reaction during the phase-separation process. In an effort to study the coupling between the kinetics of the thermodynamically driven binary phase-separation process and the connectivity-driven gelation transition[10], we have studied the phase-separation kinetics of gelatin in a poor solvent. Gelatin dissolved in a water–methanol mixture undergoes a binary phase separation into a polymer-rich phase and a polymer-poor phase as the temperature is lowered and simultaneously undergoes a reversible sol–gel transition[11]. In this paper we report the kinetics of spinodal decomposition in the gelatin–water–methanol (GWM) system and show that the occurrence of gelation has a pronounced effect on the dynamics of phase separation and on the scaling laws

* To whom correspondence should be addressed
† This represents a part of J. Lal's PhD Thesis, Boston University, 1991

0032-3861/92/142961-09

describing the time evolution of domain growth. A preliminary account of these experiments was reported earlier[12].

EXPERIMENTAL

All the experiments reported in this paper were made on swine-skin gelatin (Sigma Chemical, approximate molecular weight 50000) dissolved in a 40:60 mixture of methanol–water (by volume). It should be pointed out that, although the gelatin–water–methanol system has three components, since water and methanol are miscible they can be considered as the single solvent component and at a fixed methanol/water ratio a pseudo-binary phase diagram can be used to describe the phase separation.

Equilibrium phase diagram

The cloud-point curve and the spinodal line were determined from turbidity measurements. Samples with different concentrations of gelatin (ranging from 0.75% to 12% by weight in 100 ml solvent) were made in 1 cm path length cuvettes. For each sample the transmitted intensity from a 5 mW He–Ne laser was recorded as a function of temperature. Between each measurement the sample was heated to 313 K, which is well above the upper consolute point for this system, and thus the sample was remixed in the one-phase regime. The transmitted light intensity decreases with temperature, and this decrease is characterized by two very distinct slopes. Since the turbidity is proportional to the integral of the scattered intensity over the entire solid angle, we can interpret the temperature where the slope changes as the cloud point. Following Tanaka[11], we define the spinodal temperature as the temperature where the transmitted light intensity extrapolates to zero. For the 7.5% GWM sample used in this kinetic study, this procedure gives the spinodal and the cloud-point temperature as 303.5 K and 305 K, respectively. The phase diagram for this system appears in our earlier paper[12]. It should be pointed out that the process of gelation influences the process of phase separation, i.e. 'pins' the sample in some non-equilibrium state; thus, it is impossible to measure a true 'equilibrium' phase diagram at temperatures below the gel temperature.

Theoretical treatment of equilibrium phase diagrams in such systems with simultaneous occurrence of a sol–gel transition is given by Tanaka *et al.*[13], Coniglio *et al.*[14] and Joanny[15].

Gelation kinetics

The sol–gel transiton temperature was determined using falling-ball microviscometry. A capillary tube containing the sample and a 0.6 mm diameter steel ball was placed in a temperature-controlled bath with a glass window to observe the time of fall t_f of the ball. Since t_f is directly proportional to the shear viscosity η of the solution, the experiment shows the increase of the shear viscosity with time after a gelatin solution is quenched to a temperature T below the equilibrium sol–gel transition temperature. A sol–gel line can be obtained from these measurements by defining T_{gel} as the temperature above which the sample does not gel in finite time. Note that this is not meant to be an 'equilibrium' line. In fact, the limit to gelation may be inherently set by kinetic constraints, i.e. the rate of gelation becomes so slow that for all practical purposes the sample never gels.

Spinodal decomposition kinetics

The kinetics of phase separation was studied using the conical lens technique[16] to measure the angular dependence of the scattered light intensity at various times after the sample was quenched to a temperature in the two-phase region. The conical lens focuses light scattered at a given angle θ to a single point along the optical axis. Thus by moving a photodiode mounted on a computer-controlled linear stage we measure the angular dependence of the scattered light intensity, $I_s(k, t)$, which is proportional to the dynamic structure factor $S(k, t)$, at a fixed time t after the quench. Here $k = 4\pi n \sin(\theta/2)/\lambda$ is the scattering vector, where $\lambda = 633$ nm and $n = 1.33$ is the refractive index of the solvent. The sweep time (4 s) was small compared to the collapse time of the diffraction ring (~ 10 min). The angular resolution was $\pm 0.35°$.

The experimental procedure involved mixing the gelatin solution thoroughly in a re-entrant quartz cell (path length 0.1 mm) at 313.0 K (far above the coexistence curve and sol–gel line). The sample was then quenched to the desired final temperature by quickly transferring to a water bath held at a temperature in the spinodal region. We found that for all cases the sample equilibrated to the quench temperature in less than 15 s. For each quench we recorded both the transmitted light intensity (I_f) and the scattered light intensity ($I_s(k, t)$ at $0.5 < k < 3.5\ \mu m^{-1}$) as a function of time.

RESULTS AND DISCUSSION

Kinetics of gelation

As seen from *Figure 1a*, the viscosity $\eta \propto t_f$, the time of fall of the ball, increases by more than two orders of magnitude as one approaches the gel point. By extrapolating the inverse of the time of fall t_f to zero, we determine $\tau_{gel}(T)$, the time at which gelation occurs at temperature T. As seen from *Figure 1b*, $\tau_{gel}(T)$ increases very rapidly with increasing temperature, varying from less than a minute at 297 K to over 12 h at 304 K for the 7.5% sample. Similar behaviour is observed for the 2% sample also shown in *Figure 1b*. At any given temperature T the 2% sample takes more time to gel than the 7.5% sample. This large increase in $\tau_{gel}(T)$ as T increases during the process of physical gelation can be explained in terms of the molecular mechanism of gel formation in gelatin. The gelation process (see *Figure 2*) involves a primary process in which three random coils of gelatin associate locally forming helical regions. The helix is stabilized by hydrogen bonding of the polypeptide chains. The primary process is followed by a much slower secondary process in which there is further association of the previously developed structure. As seen in the optical rotational studies of Djabourov *et al.*[7], the primary process is exponential in time, whereas the secondary process occurs at a much slower logarithmic rate. Since we are interested in the early stages of phase-separation kinetics, the timescales involved are such that only the primary process of gelation plays any role in influencing the phase-separation kinetics.

The kinetics of the primary process can be modelled as a coil-to-helix transition[18,19]. In this model the first step involves the formation of helical regions at randomly

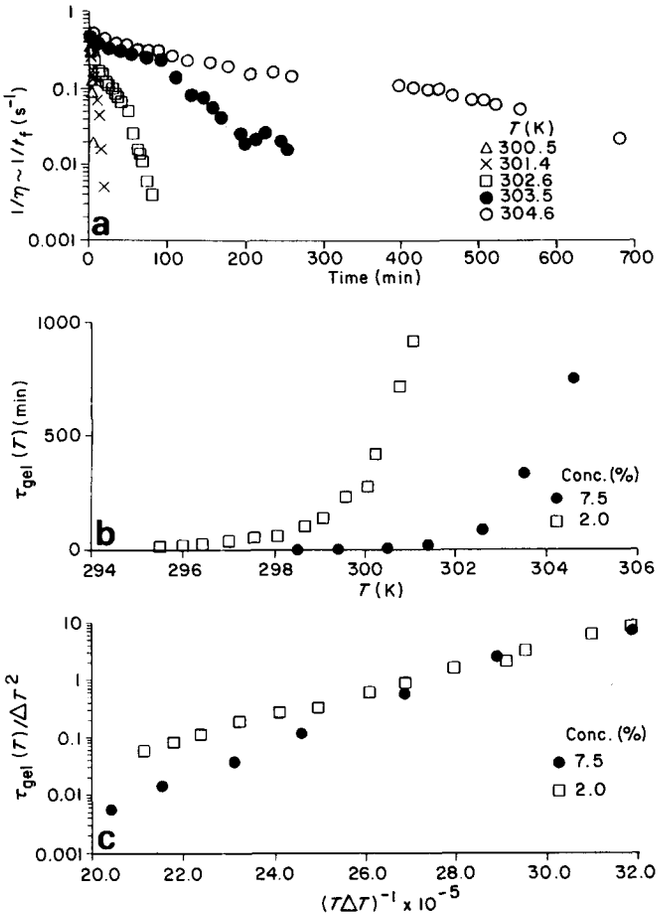

Figure 1 The results of falling-ball microviscometry measurements. (a) Inverse of the time of fall (t_f) *versus* time shown on a log scale for visual clarity at different quench temperatures T for 7.5% GWM sample. The linear plot was used to extrapolate the data to determine $\tau_{gel}(T)$, the time to gel. (b) $\tau_{gel}(T)$ *versus* temperature T (K) shown for the 7.5% and 2.0% GWM samples. (c) Semi-log plot of $\tau_{gel}(T)/\Delta T^2$ *versus* $(T\Delta T)^{-1}$ for the data in (b). Here $\Delta T = T_{gel} - T$ with $T_{gel} = 314.9$ K for 7.5% GWM sample and 311.5 K for 2.0% GWM sample

distributed sites. These act as 'nuclei' for the growth of fibrils of constant diameter, leading to the formation of a network. Godard *et al.*[19] determine the free energy of formation of the cylindrical fibrils by assuming a unidirectional growth model. By using this simple picture they can determine the surface and bulk free energy as in a nucleation process. Assuming the length of the fibril to be constant, the thermodynamic barrier of secondary nucleation is obtained by minimizing the free energy. The critical diameter of fibril formation is inversely related to the degree of undercooling $\Delta T = T_{gel} - T$, where T_{gel} is the equilibrium sol–gel transition temperature. The rate of gelation in this process is given by:

$$\log\left(\frac{\tau_{gel}(T)}{\Delta T^2}\right) = A + \left(\frac{B}{T\,\Delta T}\right) \qquad (1)$$

Here the prefactor A is related to a transport term and the constant B to the minimum energy needed for the formation of the fibril. A similar equation (a linear variation of $\log \tau_{gel}(T)$ with $1/T\,\Delta T$) was also derived by Flory and Weaver[18] in their study of the temperature dependence of viscosity of dilute collagen solutions undergoing a melting transition.

In order to apply this equation to the data shown in *Figure 1b* we need to determine T_{gel}, the equilibrium gelation temperature. (Note that because of hysteresis effects T_{gel} is not necessarily equal to T_m, the melting temperature. However, one expects the same equation to apply in gelation as in melting, as has been mentioned by Flory and Weaver[18], who noticed a small change in the gel setting temperature *versus* the measurements of gel melting.) Since, experimentally, it is hard to determine the temperature T_{gel} at which the sample never gels, because of the constraint of waiting for an infinite amount of time, we therefore estimated T_{gel} from the best fit of our experimental data to equation (1) as plotted in *Figure 1c*. For the 7.5% sample it is approximately 314.9 K and for the 2% it is 311.5 K. As expected, the higher the concentration, the faster is isothermal gelation and the higher is the upper limit of the gelation temperature. The slopes of the plots in *Figure 1c* are very similar to that obtained in the measurements of Godard *et al.*[19] in their study of gelation and melting behaviour of aqueous gelatin. In this study the slope, which represents the minimum energy needed for fibril formation, is 602 kJ mol^{-1} for the 7.5% solution and is 394 kJ mol^{-1} for the 2% sample. This indicates that the underlying mechanism governing the association or the dissociation of these triple helices is similar even though our measurements are made under poor solvent conditions.

Kinetics of spinodal decomposition

Upon quenching the sample to a temperature below the spinodal, a diffuse, weak scattering occurs, which sharpens into a well defined diffraction ring as time proceeds. As the process of phase separation proceeds, this ring grows more intense and its diameter decreases. These qualitative observations are characteristic of a spinodal process, with the diameter of the ring related to the characteristic wavevector at which growth is most pronounced.

The analysis of spinodal decomposition data is usually separated into three different time regimes, corresponding to the early, intermediate and late stages of the phase-separation process[20,21]. In the early stages of spinodal decomposition the time evolution of the concentration fluctuation δc is predicted by the linear Cahn–Hilliard[22] theory to grow exponentially, and the wavelength of the dominant mode is either constant or slowly growing if one allows for the thermal fluctuations as introduced by Cook[23]. In the intermediate stage, both the wavelength of the dominant mode of fluctuations k_m and amplitude of the fluctuations δc grow with time. In the late stage,

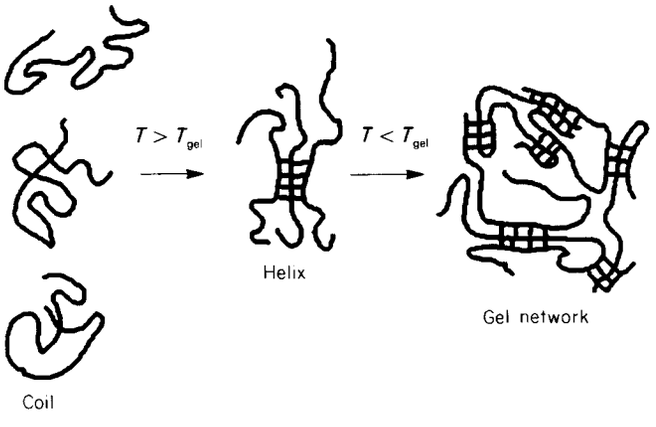

Figure 2 Schematic picture of the molecular mechanism of the sol–gel transition in gelatin. (Adapted from Harrington and Rao[29])

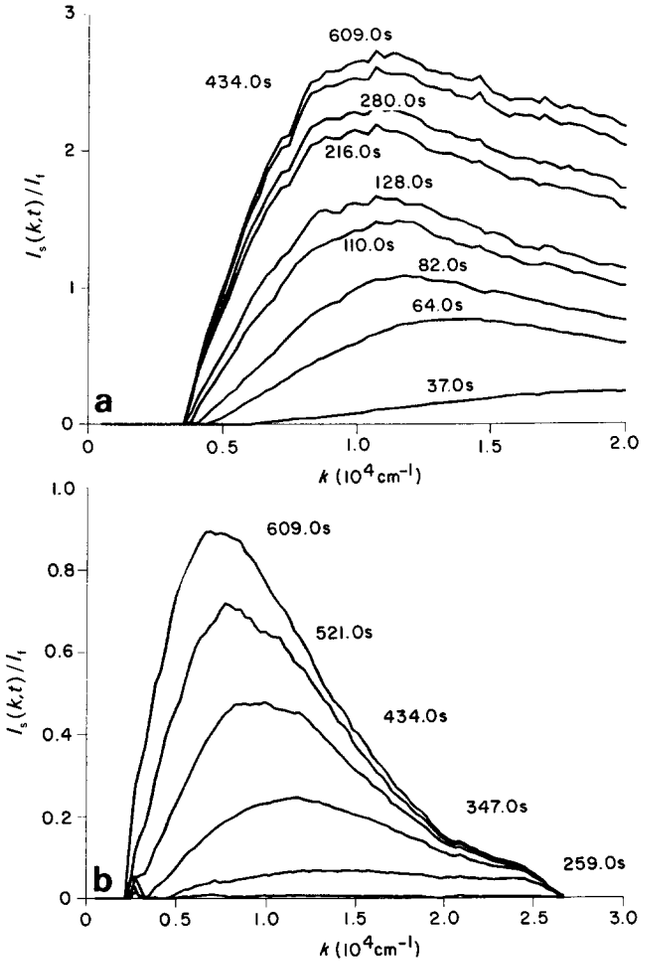

Figure 3 Time evolution of the scattered intensity $I_s(k, t)/I_f$ at different times as indicated following a quench to (a) 297.5 K and (b) 301.5 K

the amplitude of the concentration fluctuations δc reaches the equilibrium value of the concentration difference of the two coexisting phases, but the wavelength grows in a self-similar manner. It should be noted that the transitions between these three stages are not necessarily sharply defined.

Figures 3a and *3b* show a typical plot of the scattered intensity $I_s(k, t)$ *versus* the scattering vector k at different times after the 7.5% sample was quenched to 297.5 K and 302.5 K, respectively. The sharp cut-off at high k seen in *Figure 3b* arises from the edge of the conical lens. In both cases the ring initially appears at large k, and, as time proceeds, the position k_m of the maximum in $I_s(k, t)$ shifts to smaller k (i.e. the domain size increases) and I_m, the scattered intensity at $k = k_m$, grows (reflecting an increase in both domain size and concentration gradient). For the quench at 297.5 K this collapse of the diffraction ring continues until ~ 100 s after the quench. Beyond this time the peak position remains virtually unchanged, although the intensity still continues to increase. The increases of correlation length and concentration gradient with time are both signs of normal spinodal decomposition. The unusual feature seen at late times in *Figure 3a*, with the peak position remaining virtually unchanged with time, implies that the domains are 'pinned' once the sample gels. In contrast to this behaviour for deep quenches, when the sample is quenched to 302.5 K (cf. *Figure 3b*) the peak position decreases at all times, and in ~ 600 s has moved to k very close to zero. After this time the position of the scattering maximum can no longer be determined because it coincides with the transmitted beam.

A comparison of *Figures 3a* and *3b* reveals a striking difference in the shape of the structure factor at large $k > k_m$ (corresponding to structures of small size). The structure factor for the deep quench is much broader (cf. *Figure 3a*) and shows a significantly higher intensity in the 1.5–2.0 μm^{-1} range as compared with *Figure 3b*. In contrast to this high-k behaviour, the data for $k < k_m$ show the same trend at both temperatures. The much larger intensity at high k for deep quenches (e.g. 297.5 K in *Figure 3a*) may indicate that a second structure is growing at large k. Such a structure could arise from inhomogeneities on a small length scale due to crosslinking and network formation. Although a second peak cannot be established over the limited range of k examined in this study, the data do suggest some structure growing after the onset of gelation. In a recent study of a hydrogen-bonded polymer blend, He *et al.*[24] have found a two-peaked structure in spinodal decomposition with one of the peaks growing at fixed wavevector. In their work the fixed peak was at a lower k than the moving peak. Since the hydrogen-bonded groups in the blend were very low in concentration, they may have generated a very large length scale structure. In our work, the hydrogen-bonded groups are very high in concentration and thus the hydrogen-bonded network structure is formed on a very short length scale. Even though this interpretation is at the present time speculative, a further examination of the secondary structure formed in systems capable of crosslinking during spinodal decomposition may lead to clarification of this point.

Figure 4a shows log–log plots of k_m *versus* time for different quench temperatures. All of the quenches show a region of power-law behaviour $k_m \sim t^{-\alpha}$, but the value of α and the range over which power-law behaviour is observed depends on the quench depth. For the deepest quench data at 297.5 K there is a sudden transition from a power-law growth in the early stages, $k_m \sim t^{-0.6}$, to k_m becoming constant in time for $t > t_{final}$. The data for the intermediate quenches at 299.5 and 300.5 K show a gradual crossover from power-law growth to pinned domains, whereas data for the shallowest quenches at 301.5 and 302.5 K show power-law behaviour over the entire time observable in this experiment.

Figure 4b and *4c* show the temperature dependence of the characteristic domain size k_{final}^{-1} and the time t_{final} at which the domains are pinned. The temperature dependence of t_{final} is very similar to that of $\tau_{gel}(T)$ (cf. *Figure 1b*), suggesting that the process of gelation is responsible for the pinning of the phase-separating domains. The large dependence of k_{final} on T suggests that the coupling of phase separation and gelation controls the ultimate size of the domain ($\propto k_{final}^{-1}$). As seen here, (i) the final wavevector k_{final} at which domain growth stops increases as the quenches become deeper and (ii) the domain growth appears to stop at earlier times (t_{final}) for deeper quenches.

For normal spinodal decomposition, without gelation, one usually observes power-law scaling, $k_m \sim t^{-\alpha}$ and $I_m \sim t^{\gamma}$, in the late stages of growth. In the GWM system, as discussed above, we observe power-law growth of the domain size. To see whether the growth in peak intensity prior to the onset of gelation follows a power law, we

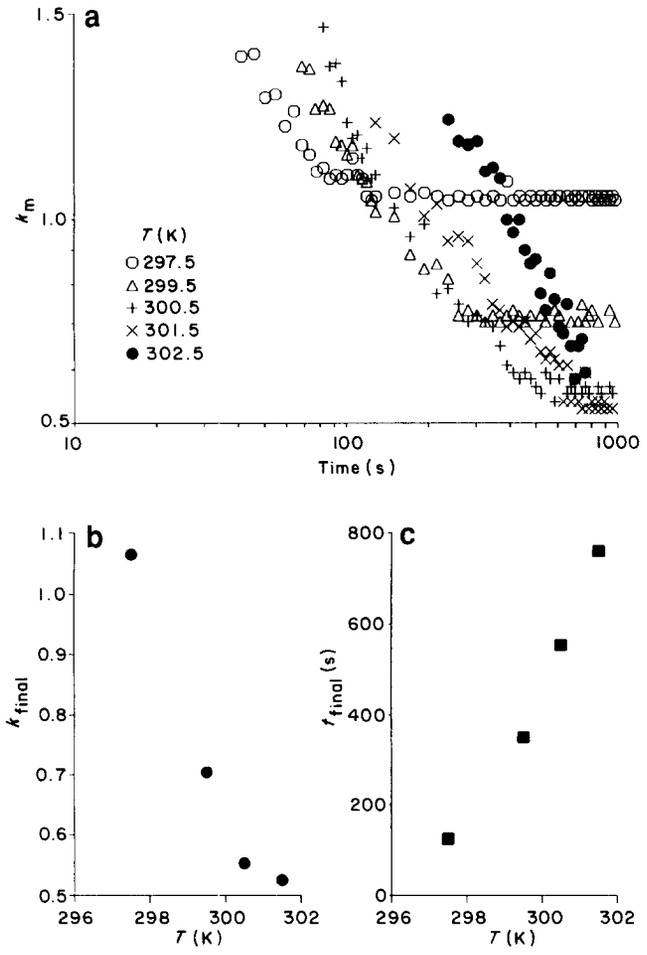

Figure 4 (a) Time dependence of k_m (in units of 10^4 cm^{-1}) at different quench temperatures T as indicated in the figure. (b) The wavevector at which domain growth stops, k_{final} (in units of 10^4 cm^{-1}), as a function of the quench temperature T. (c) The final time t_{final} as a function of quench temperature T

plot the intensity at the peak normalized by the forward intensity I_m/I_f on a log–log scale in *Figure 5a*. An examination of *Figure 5a* reveals a very rapid initial growth followed by a crossover to a slower growth at later times. The crossover occurs in the vicinity of t_{final}. It is evident from the figure that no clear region of power-law growth in intensity with a temperature-independent exponent γ can be identified, even for $t < t_{final}$. This would imply that the data for $t < t_{final}$ are in the early to intermediate stages of spinodal decomposition[25].

The slow growth in intensity beyond t_{final} can be better seen in *Figure 5b*, which shows the data in *Figure 5a* for deep quenches on a linear plot. We note that the data for $t > t_{final}$ can be fitted quite well to an equation of the form:

$$I_m = I_{final}(1 - e^{-\beta t})$$

The actual calculated values are plotted in *Figure 5b* (smooth curves). Such an equation has been proposed to describe the kinetics of helix formation as measured by optical rotation techniques[17]. If we postulate that beyond t_{final} the growth of scattered intensity is not due to the increase in the size of domains and concentration fluctuations due to phase separation, but rather due to increase in the extent of network formation in the phase-separated domains arising from further cross-linking, then the scattered intensity reflects the increase in the number of crosslinked helical regions and hence may follow the same law.

It is possible to analyse the data for $t < t_{final}$, where we observe initial rapid growth in intensity in terms of the early-time Cahn–Hilliard[22] and Cook[23] (CHC) theory for spinodal decomposition kinetics. The validity of the linear theory holds for a longer time in the vicinity of the spinodal owing to the slowing down of the diffusive process (cf. *Figure 3b*). According to the linear CHC theory, the scattered intensity is given as:

$$I_s(k, t) = I_\infty + (I_0 - I_\infty)e^{2R(k)t} \quad (2)$$

where

$$R(k) = Dk^2\left(1 - \frac{k^2}{2k_m^2(0)}\right) \quad (3)$$

and I_0 and I_∞ are related to the initial structure factor and the virtual structure factor corresponding to the final state. As discussed by He *et al.*[24] at very early times the contribution of the virtual structure factor is negligible and the above equation then reduces to the Cahn–Hilliard form[22]. Also our calculations for polymer solutions show that, although the Cook term causes the peak position

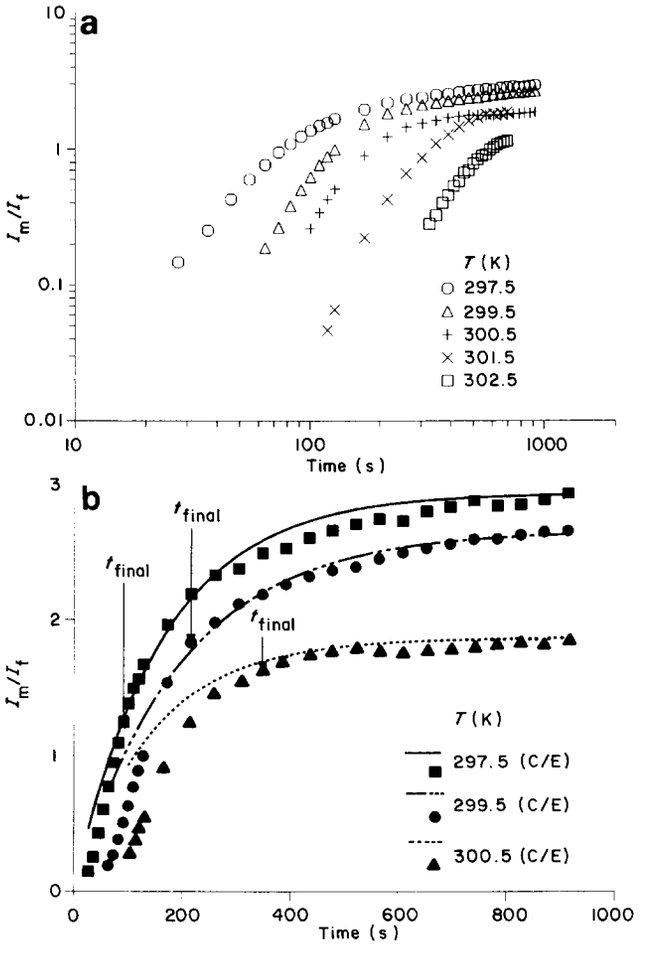

Figure 5 (a) Log–log plot of intensity I_m/I_f *versus* time at different quench temperatures T. (b) The data of (a) plotted on a linear graph. The symbols correspond to the experimental data at different temperatures as indicated and the curves show the fitted form $I_m = I_{final}(1 - e^{-\beta t})$, where $\beta = 6.2 \times 10^{-3}$, 5.1×10^{-3} and 6.8×10^{-3} s^{-1}, and $I_{final} = 2.92$, 2.65 and 1.87 for the temperatures 297.5, 299.5 and 300.5 K respectively

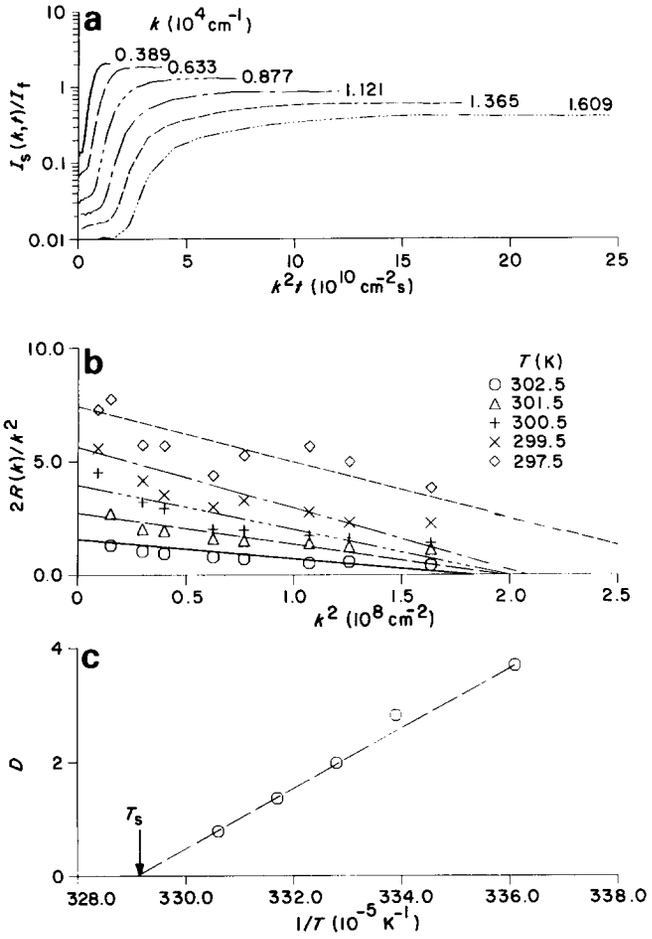

Figure 6 (a) The scattered intensity $I_s(k, t)$ as a function of k^2t for selected values of k. (b) The initial growth rate $R(k)$ determined from the slope of the linear portion of (a) is plotted as $R(k)/k^2$ (in units of 10^{-10} cm^2 s^{-1}) *versus* k^2. (c) The initial diffusion constant D (in units of 10^{-10} cm^2 s^{-1}), obtained as discussed in the text, *versus* the inverse quench temperature. The data extrapolated to $D = 0$ give a good estimate of the spinodal temperature T_s for the 7.5% sample

to shift in right from the beginning, the increase of intensity for very early times is almost exponential[26]. These calculations thus suggest that the extrapolated growth rate at zero time and hence the initial diffusion constant for the phase-separation process can be determined by neglecting the I_∞ term in equation (2).

From semi-log plots of scattered intensity *versus* k^2t (cf. *Figure 6a*) we can calculate the initial growth rate:

$$R(k)/k^2 = D[1 - k^2/2k_m^2(0)]$$

The results of such a calculation are shown in the $R(k)/k^2$ *versus* k^2 plots of *Figure 6b*. The decrease of the initial slope of $R(k)/k^2$ with increasing k^2 is clearly seen at small k in *Figure 6b*. In order to determine D from this information we follow the approach used for polymer blends[21], and extrapolate the linear region in $R(k)/k^2$ *versus* k^2 plots to $k = 0$ to determine D at $t = 0$ from the y intercept and similarly determine the initial wavevector $k_m(0)$ from the x intercept. The rate of phase separation at any given temperature is $\tau_0^{-1} = Dk^2$. As expected, the rate of phase separation is faster for deeper quenches and becomes very small for shallow quenches with $D = 0$ for $T = T_s$. The temperature dependence of D is shown in *Figure 6c*. By extrapolating these data we obtain $T_s = 303.9$ K for the 7.5% sample, which also agrees well with T_s determined using the turbidity measurements discussed earlier[12].

The late-stage growth where power-law scaling and dynamic scaling hypotheses are applicable is not observed here because of the onset of gelation for deep quenches. This behaviour is in contrast to that seen in experiments in polymer solutions[7,25,26] and blends[20,21], where late-stage kinetics can be readily seen in light scattering experiments for deep quenches. According to the dynamic scaling hypothesis the structure factor data plotted as $I_s(k, t)k_m^3/I_f$ *versus* k/k_m should collapse to a universal time- and temperature-independent form[2].

As shown in *Figure 7a* for the 297.5 K quench the structure factor data do not collapse to a single curve. Similar results were obtained also for the other two deep quenches (299.5 and 300.5 K). For the shallow quench data (301.5 and 302.5 K) gelation does not appear to play a significant role in the time range of our measurements. However, we found that even there these data do not collapse to a single curve as shown in *Figure 7b*. The reason for this non-universal behaviour for shallow quenches is that the rate for the phase-separation process becomes slow and the characteristic length scale becomes very large (τ_0^{-1} and $k \to 0$ as $T \to T_s$). Thus by the time the phase-separation process reaches the conditions appropriate to see late-stage growth, the peak of the structure factor is very close to $k = 0$ and is obscured by the transmitted beam. Similar non-universality for shallow quenches was observed in our previous work on spinodal decomposition in polystyrene–cyclohexane[25] solutions.

Influence of gelation on phase separation

Our data show a very pronounced dependence of kinetics of spinodal decomposition on the quench temperature. For shallow quenches the results are similar to that seen in other polymer solutions. In contrast, the

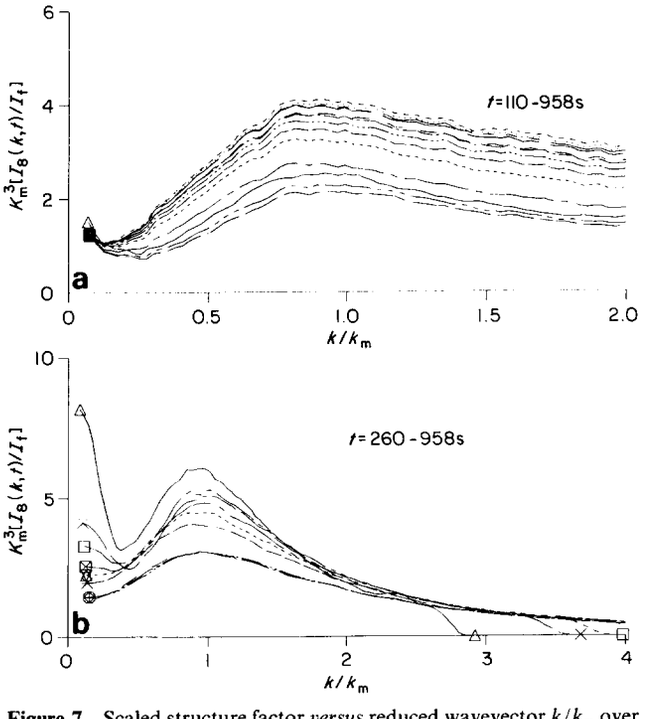

Figure 7 Scaled structure factor *versus* reduced wavevector k/k_m over the range of times indicated for quench to (a) $T = 297.5$ K and (b) $T = 301.5$ K

data for deep quenches show a cessation of growth before the phase-separation process has gone to completion, and the sample is pinned in some metastable state with microphase-separated domains. In an effort to understand these differences, we suggest that when gelation and phase separation occur simultaneously the kinetics and morphology depend on the location of T relative to T_s and T_{gel} *as well as* on the rates of phase separation and gelation τ_0^{-1} and τ_{gel}^{-1}, respectively. When $T > T_{gel}$ then the phase separation should be virtually independent of gelation and the sample should phase-separate into two macroscopically distinct components. When $T < T_{gel}$ and $\tau_0^{-1} \gg \tau_{gel}^{-1}$ then the sample separates into two phases before any gelation occurs and subsequently one or both of these phases gels. When $T < T_{gel}$ and $\tau_0^{-1} \lesssim \tau_{gel}^{-1}$ then the two processes are coupled. In this case, as soon as the sample is quenched, the process of phase separation starts creating domains rich in polymer and poor in polymer. At any given temperature, the polymer-rich domains gel faster than the polymer-poor regions. Hence the polymer-poor regions keep growing until they encounter the infinite viscosity of the polymer-rich phase, which leads to the locking of domains and the pinning of the wavevector at a particular k_{final}. Since the rates of gelation and phase separation both increase with increasing quench depth (see *Table 1*), it follows that the system becomes pinned at earlier times, and with smaller characteristic domain size (i.e. larger k_{final}) for deeper quenches.

We put this idea to a quantitative test in the following way. In the absence of gelation, the size of the phase-separating domains grows as $k_m \sim t^{-\alpha}$. Using the characteristic length scale and timescale relevant to the quench temperature, we get $k/k_m(0) \sim (t/\tau_0)^{-\alpha}$. If we substitute the experimentally determined $t = \tau_{gel}$, the time at which the sample gels at the temperature T, we can calculate the wave number κ_{final} at which domain growth stops. Using equation (1) for the temperature dependence of τ_{gel} we can also write:

$$\frac{\kappa_{final}}{k_m(0)} = c_0\left(\frac{\tau_{gel}}{\tau_0}\right)^{-\alpha} = c_0\left(\frac{1}{\tau_0}\right)^{-\alpha} \exp\left(-A\alpha - \frac{B\alpha}{T\,\Delta T}\right) \quad (4)$$

The values of A, B and ΔT determined by fitting the gelation kinetics data (see *Figure 1c*) and the values of $k_m(0)$ and τ_0 obtained from the Cahn–Hilliard analysis (see *Table 1*) are used to calculate the predicted values of κ_{final}. Note that there is a proportionality constant c_0, which is determined by forcing the measured k_{final} and calculated κ_{final} to coincide at 297.5 K. Using this constant we can predict the value of κ_{final} at other temperatures. These results for different quench temperatures are shown in *Table 1*. We see from *Table 1* that, although the temperature-dependent trend of k_{final} is qualitatively well reproduced by equation (4), the quantitative agreement is not very good. This is not surprising given the vastly simplistic nature of the

Table 1 The results of the linear Cahn–Hilliard analysis prior to the onset of gelation and the experimentally measured final wavevector k_{final} at which the phase-separated domains are pinned. The results of using equation (4) to calculate κ_{final} are also given. The macroscopic gel time τ_{gel} determined by falling-ball viscometry at each temperature is also given. The initial diffusion constant D is in units of 10^{-10} cm^2 s^{-1} and $k_m(0)$, k_{final} and κ_{final} are in units of 10^4 cm^{-1}

T (K)	$k_m(0)$	D	τ_{gel} (min)	τ_0 (s)	κ_{final}	k_{final}
302.5	0.96	0.78	88.0	139.1	0.17	–
301.5	0.99	1.36	22.0	75.0	0.26	0.52
300.5	1.00	1.98	8.0	50.5	0.39	0.55
299.5	1.02	2.82	3.5	34.1	0.54	0.70
297.5	1.23	3.70	1.0	17.9	1.06[a]	1.06

[a]See text for a discussion of this point

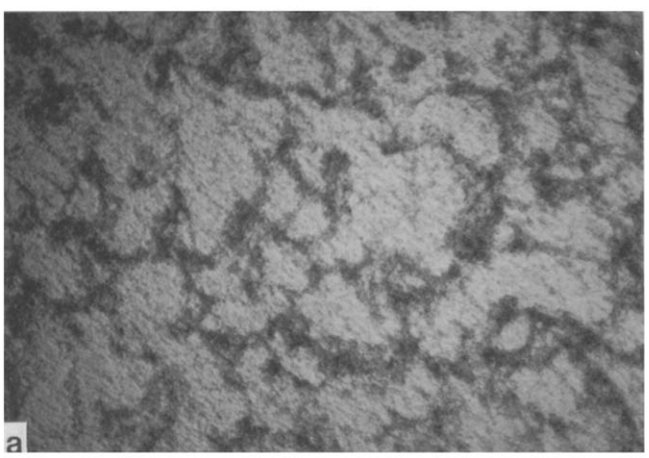

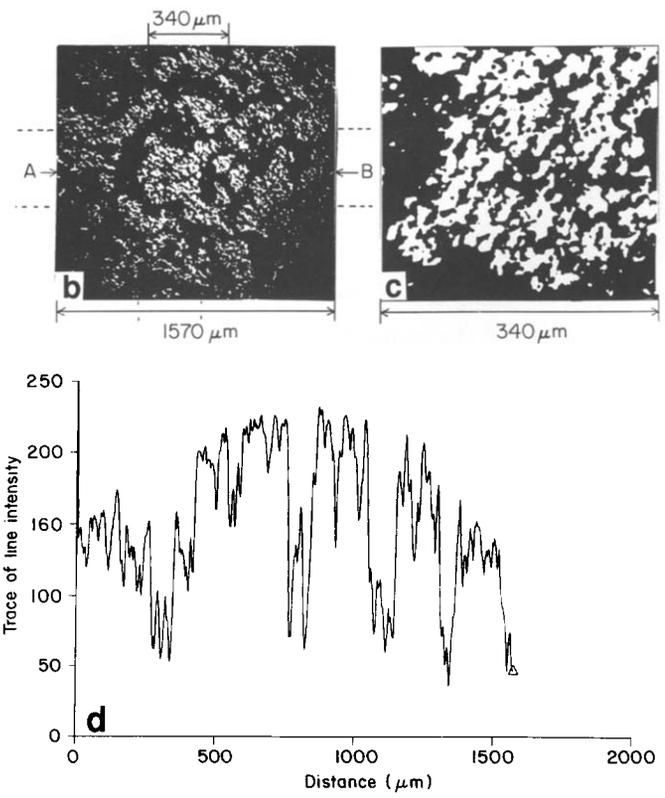

Figure 8 (a) Optical micrograph with a magnification of 40× showing the morphology of the phase-separated domains from a GWM sample that was quenched to room temperature. (b) Digitized image of part of the micrograph in (a). The overall size of the picture is 1570 × 1570 μm^2. (c) A higher-magnification image of the low-contrast region demarcated by the broken lines in (b). Overall size of the magnified region is 340 × 340 μm^2 with black and white regions of 10–12 to 30–55 μm, respectively. (d) Trace of line intensity *versus* distance across the line AB as indicated in (b).

arguments used to obtain equation (4). Furthermore, the determination of $k_m(0)$ and τ_0 from Cahn–Hilliard analysis is subject to large errors because of the very small range over which exponential growth is seen.

It is also possible that τ_{gel} obtained from falling-ball viscometry experiments corresponds to the formation of a network on a macroscopic scale (~ 1 mm), whereas phase-separated domain growth stops on a microscopic length scale (10–200 μm), which may occur at a different time $\tau_{microgel} \neq \tau_{gel}$. This would cause κ_{final} calculated using τ_{gel} to be different than that measured in the spinodal decomposition experiment.

The influence of gelation on phase separation is borne out by *Figure 8a*, which shows a micrograph of the phase-separated domains after the sample was quenched to room temperature. The micrograph, taken with a magnification of 40 × with an optical microscope, reveals the network structure and well formed domains of high and low contrast. The dark regions are rich in gelatin and the low-contrast regions are poor in gelatin. The average domain size of the gelatin-rich regions is 132 μm with sizes ranging from 96 to 180 μm, and that of the gelatin-poor regions is 283 μm with sizes ranging from 180 to 336 μm. The overall connected morphology of the gelatin-rich phase arises due to spinodal decomposition. Since the sample does not phase-separate fully into two distinct phases, the early stage percolating structure characteristic of the spinodal decomposition process is pinned owing to the onset of gelation. *Figure 8b* reveals that the low-contrast regions corresponding to the polymer-poor region in *Figure 8a* also show a fibrillar network-like structure on a smaller length scale (~ 10 times smaller). The overall size of the magnified region shown in *Figure 8b* is 340 μm with the black regions corresponding to gelatin fibres of size 10–15 μm and white regions corresponding to domains of size 30–50 μm consisting of mostly solvent. *Figure 8c* shows a typical trace of the intensity along a line. The gelatin-rich regions correspond to the minimum values of intensity, the fibres in the polymer-poor region give rise to secondary minima, while the regions of mostly solvent show the highest value of intensity. Since the decrease in intensity in any region is proportional to the amount of gelatin, the presence of gelatin in the low-contrast region is smaller compared to that in the polymer-rich region as indicated by relative amounts of the dips in the trace. It should be noted that the intermediate stage morphology seen here is very different from that seen in liquid–liquid phase separation[27] and in polystyrene–cyclohexane solutions[28], where we observe the true late stages, i.e. the break-up of the initial connected structure and the coalescence of the droplets.

The structure of the gel network involving the formation of local helical regions can only be seen in electron micrographs of gelatin[17], which also show a self-similar structure. It thus appears that the phase-separated network structures of a gel can be characterized at several different length scales and appear to be self-similar.

SUMMARY

In conclusion, we note that, in spite of the qualitative similarity with other systems, the dynamical behaviour in gelatin solution differs in several important ways from the dynamics in either small-molecule mixtures or polymer–polymer mixtures. These are summarized below.

(i) The dynamic behaviour depends on the location of the quench temperature T relative to the equilibrium sol–gel transition temperature T_{gel} and also on the relative magnitudes of the time taken for gelation (τ_{gel}) and the time taken for the phase separation to occur (τ_0). For the case where $\tau_{gel} \gg \tau_0$, the dynamics is essentially the same as that observed in dilute polymer solutions with a power-law relationship $k_m \sim t^{-0.6}$ seen in early times. Interestingly, this behaviour is observed even when the quench temperature is less than T_{gel}, the equilibrium sol–gel transition temperature, suggesting that, if the rate of the gelation process is very slow compared to the phase-separation process, then it has virtually no influence on phase-separation dynamics. However, when the sample is quenched to a temperature below T_{gel} and $\tau_{gel} \sim \tau_0$ or $\tau_{gel} < \tau_0$, the spinodal decomposition process does not go to completion. The phase-separation process produces domains that grow to some finite size and then get pinned. The deeper the quench into the gel phase, the earlier in time is the onset of gelation and the larger is the final wavevector (i.e. the smaller the domain size) at which the morphology becomes pinned.

(ii) An unusual behaviour is observed in the growth of the intensity. In early stages we observe exponential growth as expected from the Cahn–Hilliard theory, followed by a slow growth with the intensity growing to a saturation limit. For deep quenches the slow growth in intensity observed at late times can be fitted to an equation of the form $I_m = I_{final}(1 - e^{-\beta t})$, which reflects the effects of crosslinking on the phas-separated domains.

(iii) The large dependence of k_{final} on temperature reflects the effects of both phase separation and gelation and is controlled by the relative rates of these two time-dependent processes. Using the initial rates of phase separation calculated from the Cahn–Hilliard analysis and τ_{gel} obtained from viscosity measurements, we can predict the dependence of k_{final} on temperature. This relationship provides a semi-quantitative approach to determining the domain size at which the network is pinned by varying the temperature and thus has a potential application in processes such as immersion precipitation used for preparation of polymeric membranes by immersion of a wet film into a non-solvent[6]. Our results suggest that temperature can be used as a very sensitive variable to control morphology and pore size in the process of immersion precipitation.

(iv) The phase-separated domains reveal a connected structure on length scales of several hundred micrometres superimposed on a finer network structure due to gelation seen under higher magnification. A further study of this network structure and the time evolution of the morphology needs to be pursued.

ACKNOWLEDGEMENTS

This research was supported by grants from NSF and British Petroleum.

REFERENCES

1 Goldburg, W. E. 'Scattering Techniques Applied to Supramolecular and Nonequilibrium Systems' (Eds. S. H. Chen, B. Chu and R. Nossal), Plenum Press, New York, 1980, and references therein

2 Gunton, J. D., San Miguel, M. and Sahni, P. S. 'Phase Transitions and Critical Phenomena' (Eds. C. Domb and J. L. Lebowitz), Vol. 8, Academic Press, London, 1983, p. 267
3 Jackson, C. L. and Shaw, M. T. *Polymer* 1990, **31**, 1070
4 Boyer, R. F., Baer, E. and Hiltner, A. *Macromolecules* 1985, **18**, 427
5 Reuvers, A. J., Altena, F. W. and Smolders, C. A. *J. Polym. Sci.* 1986, **24**, 793
6 van Aarsten, J. J. and Smolders, C. A. *Eur. Polym. J.* 1970, **6**, 1105
7 Bansil, R. and Lal, J. Extended Abstracts, 'Fractal Aspects of Materials: Disordered Systems' (Eds. D. A. Weitz, L. M. Sanders and B. B. Mandelbrot), Materials Research Society, Pittsburgh, 1988, EA-17, p. 255; Lal, J. and Bansil, R. 'Fractal Aspects of Materials—1989' (Eds. J. H. Kaufman, J. E. Martin and P. W. Schmidt), Materials Research Society, Pittsburgh, 1989, EA-30, p. 11
8 Otake, K., Inomata, H., Yagi, Y., Konno, M. and Saito, S. *Polym. Commun.* 1989, **30**, 204
9 Hashimoto, T., Takenaka, M. and Jinnai, H. *Polym. Commun.* 1989, **30**, 177
10 Stauffer, D., Coniglio, A. and Adam, M. *Adv. Polym. Sci.* 1982, **44**, 103
11 Tanaka, T., Swislow, G. and Ohmine, I. *Phys. Rev. Lett.* 1979, **42**, 1556
12 Bansil, R., Carvalho, B. and Lal, J. 'Alloy Phase Stability' (Eds. G. M. Stocks and A. Gonis), Kluwer, Dordrecht, 1989, p. 639
13 Tanaka, F. and Matsuyama, A. *Phys. Rev. Lett.* 1989, **62**, 2759; Tanaka, F. *Macromolecules* 1990, **23**, 3790
14 Coniglio, A., Stanley, H. E. and Klein, W. *Phys. Rev.* (*B*) 1982, **25**, 6805
15 Joanny, J. F. *Polymer* 1980, **21**, 71
16 Pine, D. J. *Rev. Sci. Instrum.* 1984, **55**, 856
17 Djabourov, M., Leblond, J. and Papon, P. *J. Phys. Fr.* 1988, **49**, 319
18 Flory, P. J. and Weaver, E. S. *J. Am. Chem. Soc.* 1960, **82**, 4518
19 Godard, P., Biebuyck, J. J., Daumerie, M., Naveau, H. and Mercier, J. P. *J. Polym. Sci.* 1978, **16**, 1817
20 Hashimoto, T., Itakura, M. and Hasegawa, H. *J. Chem. Phys.* 1986, **85**, 6118; Hashimoto, T., Itakura, M. and Shimidzu, N. *J. Chem. Phys.* 1986, **85**, 6773; for a recent review see, Hashimoto, T. in 'Phase Transitions', Vol. 12, Gordon and Breach, New York, 1988, pp. 42–119
21 Wiltzius, P., Bates, F. S. and Heffner, W. R. *Phys. Rev. Lett.* 1988, **60**, 1538; Bates, F. S. and Wiltzius, P. *J. Chem. Phys.* 1989, **91**, 3258
22 Cahn, J. W. and Hilliard, J. H. *J. Chem. Phys.* 1958, **28**, 258
23 Cook, H. E. *Acta Metall.* 1970, **18**, 297
24 He, M., Liu, Y., Feng, Y., Jia, M. and Han, C. C. *Macromolecules* 1991, **24**, 464
25 Lal, J. and Bansil, R. *Macromolecules* 1991, **24**, 290
26 Lal, J. PhD Thesis, Boston University, 1991
27 Guenoun, P., Gastaud, R. Perrot, F. and Beysens, D. *Phys. Rev.* (*A*) 1987, **36**, 4876
28 Lal, J. and Pajevic, S. Late stage morphology of phase separation in polystyrene–cyclohexane solution, Unpublished data
29 Harrington, W. F. and Rao, N. V. *Biochemistry* 1970, **9**, 3714